Supporting Information

Reconfigurable Multi-State Optical Systems Enabled by VO_2 Phase Transitions

Xiaoyang Duan,[1] Samuel T. White,[2] Yuanyuan Cui,[3] Frank Neubrech,[1] Yanfeng Gao,[3,] Richard F. Haglund,[2,4,*] Na Liu[5,6,*]*

[1]Max Planck Institute for Intelligent Systems, Heisenbergstrasse 3, 70569 Stuttgart, Germany
[2]Department of Physics and Astronomy, Vanderbilt University, Nashville, TN 37212, USA.
[3]School of Materials Science and Engineering, Shanghai University, Shanghai 200444, China.
[4]Interdisciplinary Materials Science Program, Vanderbilt University, Nashville, TN 37212, USA.
[5]2nd Physics Institute, University of Stuttgart, Pfaffenwaldring 57, 70569 Stuttgart, Germany
[6]Max Planck Institute for Solid State Research, Heisenbergstrasse 1, 70569 Stuttgart, Germany
*E-mail: na.liu@pi2.uni-stuttgart.de, richard.haglund@vanderbilt.edu, yfgao@shu.edu.cn.

Including:

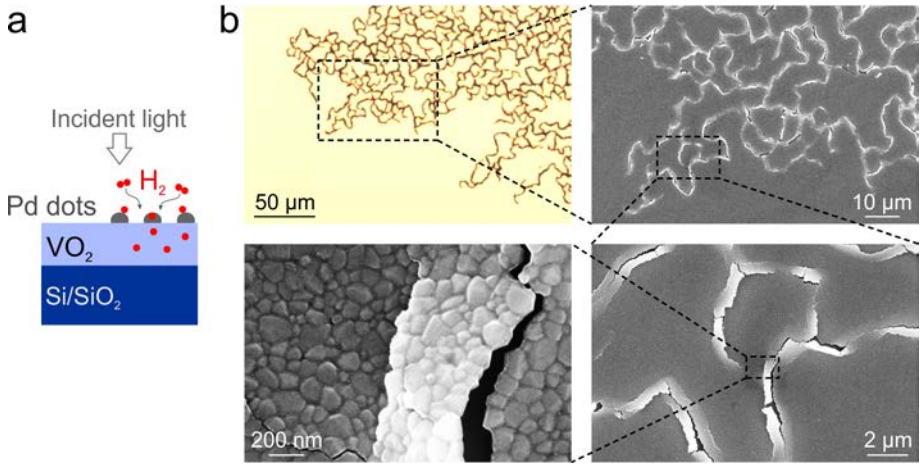

Figure S1 | a, Schematic of the VO_2 (60 nm)/silicon substrate. **b,** Optical and SEM images of the sample after hydrogenation for 1 hour at 100 °C. The film shows clear damage to the VO_2 film due to lattice expansion with increasing H content.

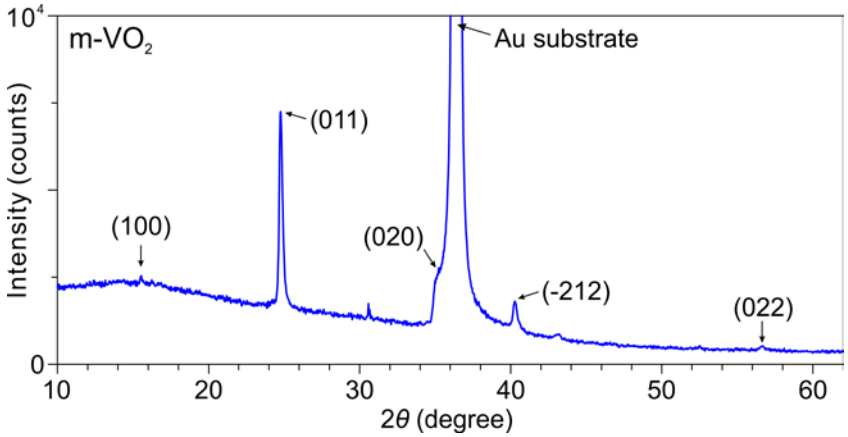

Figure S2 | X-ray diffraction of the as-prepared m-VO_2 film deposited on Au (100 nm)/Si substrate measured at room temperature under ambient condition. The strongest peak appears at 2θ = 27.6°, corresponding to the (011) planes of m-VO_2. This shows the preferred growth orientation of VO_2 on the gold substrate, consistent with previous studies.[1]

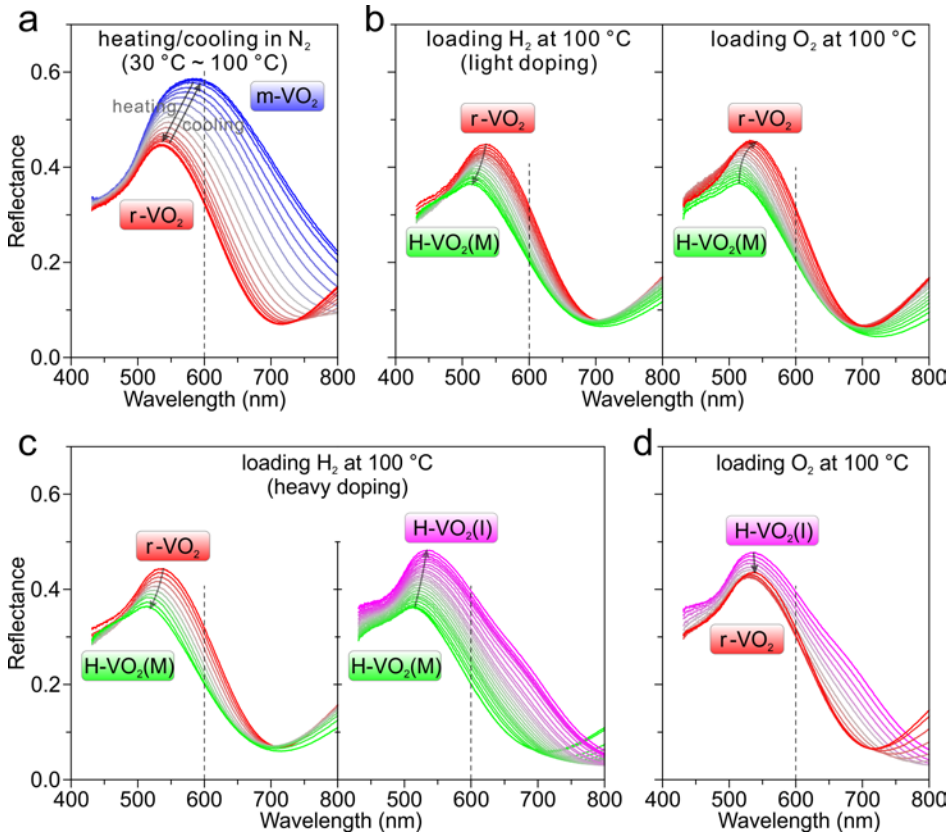

Figure S3 | Evolution of measured reflectance spectra of the VO_2 sample in four different states. Reflectance at 600 nm (highlighted by the black-dashed lines) is tracked to indicate the phase transition paths. **a**, IMT between the m-VO_2 and r-VO_2 states through temperature tuning. **b**, Light hydrogenation from r-VO_2 to H-VO_2(M), and subsequent dehydrogenation from H-VO_2(M) to r-VO_2. **c**, Heavy hydrogenation from r-VO_2 to H-VO_2(I) via H-VO_2(M). **d,** Dehydrogenation from H-VO_2(I) to r-VO_2, by completely skipping H-VO_2(M).

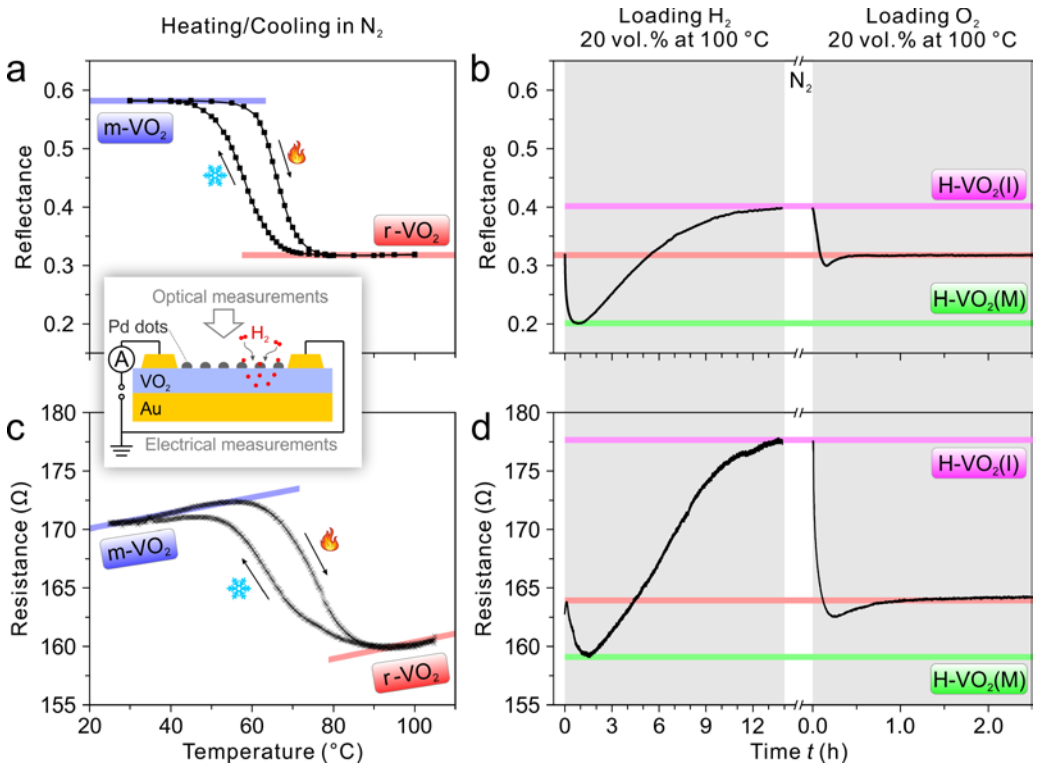

Figure S4 | *In situ* optical (**a**,**b**) and electrical (**c**,**d**) measurements of the VO_2 sample. Inset: schematic of the measurement configuration. The applied voltage was kept at 50.00 ± 0.01 mV.

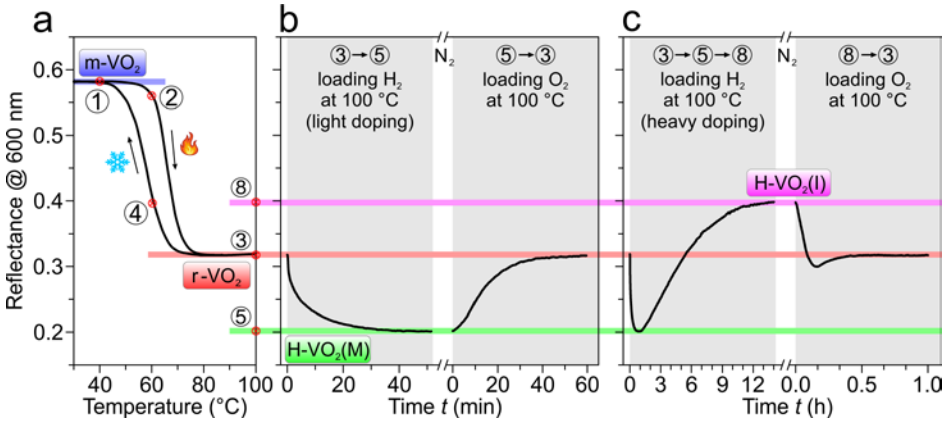

Figure S5 | *In situ* reflectance spectroscopy during hydrogen loading and unloading at 100 °C. The temperature-dependent hysteresis curves from Fig. 1c of the main text are replotted in (**a**) for a direct comparison. At different gas loading times, VO_2 is (**b**) lightly hydrogenated to H-VO_2(M), following the path '③→⑤', and (**c**) heavily hydrogenated to H-VO_2(I), following the path '③→⑤→⑧'.

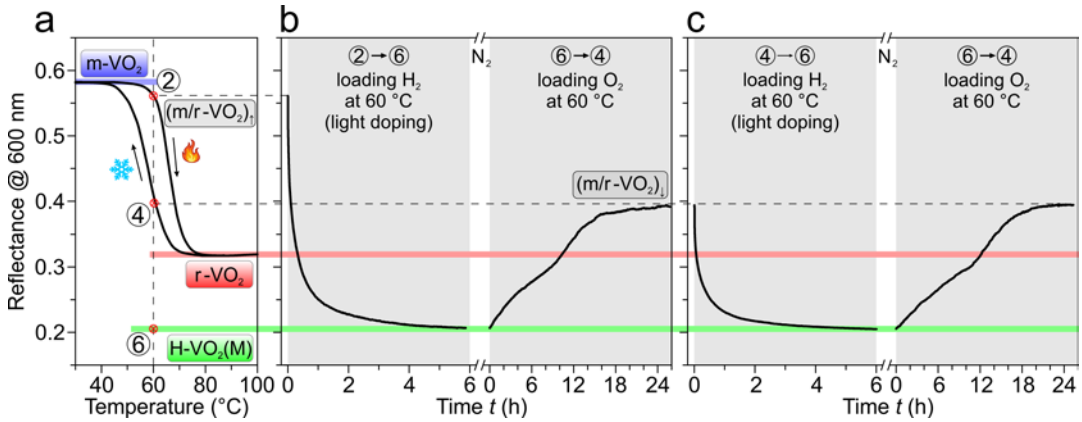

Figure S6 | *In* situ reflectance during hydrogen loading and unloading at 60 °C. H-doping of the (**b**) (m/r-VO_2)↑ state ('②') or the (**c**) (m/r-VO_2)↓ state ('④') results in the formation of H-VO_2(M). Upon O_2 exposure, state '④' is restored.

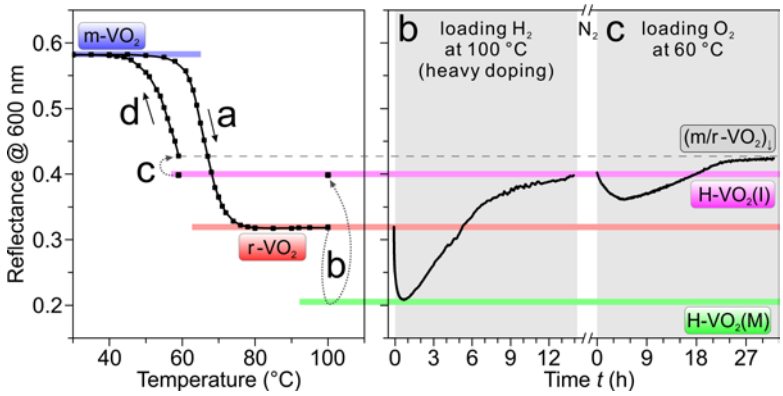

Figure S7 | Dehydrogenation of H-VO_2(I) at 60 °C. **a**, With increasing the temperature from 30 °C to 100 °C stepwise in pure N_2, the IMT from m-VO_2 to r-VO_2 is visualized. **b**, Loading H_2 gas at 100 °C. The sample is lightly hydrogenated to H-VO_2(M) first, and then heavily hydrogenated to H-VO_2(I). When the sample reaches H-VO_2(I) completely, the temperature is decreased to 60 °C. **c**, Loading O_2 gas at 60 °C. First, the reflectance decreases. It indicates that dehydrogenation starts. Then, the reflectance increases and is stabilized at the (m/r-VO_2)↓ state (gray-dashed line). **d**, Decreasing the temperature to 30 °C in pure N_2. The reflectance is restored to m-VO_2 along the hysteresis curve.

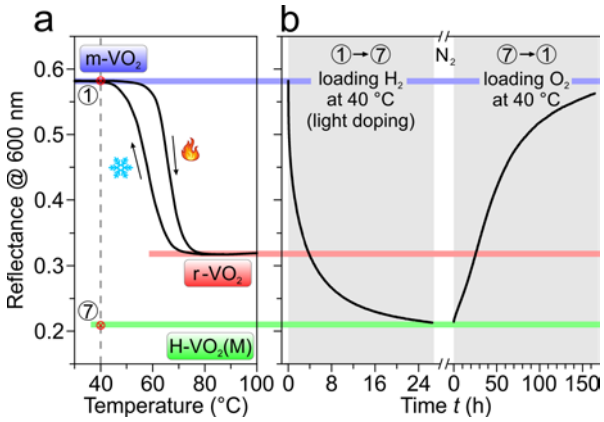

Figure S8 | *In situ* reflectance during hydrogen loading and unloading at 40 °C.

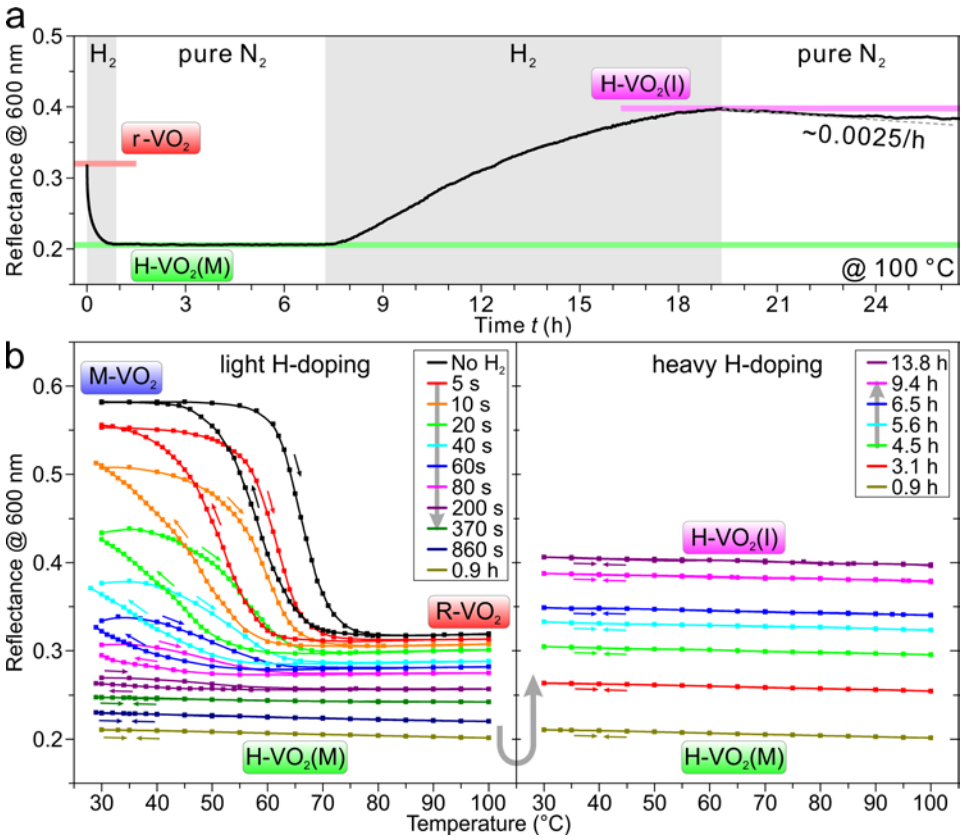

Figure S9 | a, H-VO_2(M) and H-VO_2(I) can be maintained by switching off H_2 for several hours at 100°C. They are quite stable in pure N_2 even at high temperatures. **b**, Hysteresis of the VO_2 IMT in dependence on hydrogen loading time *t*. After hydrogen exposure at 100 °C for a certain time *t*, the hysteresis of the H-VO_2 is carried out by temperature tuning in pure nitrogen.

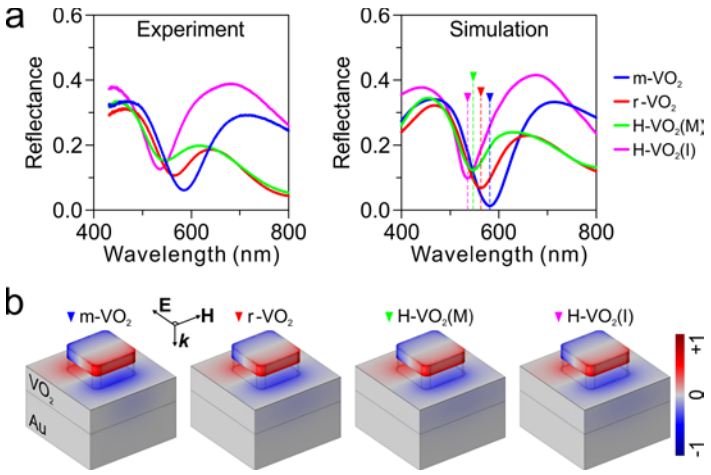

Figure S10 | a, Experimental and simulated reflectance spectra of the colour square with D = 118 nm and g = 100 nm at the four different states. **b**, Simulated surface charge distributions at resonance at the four different states.

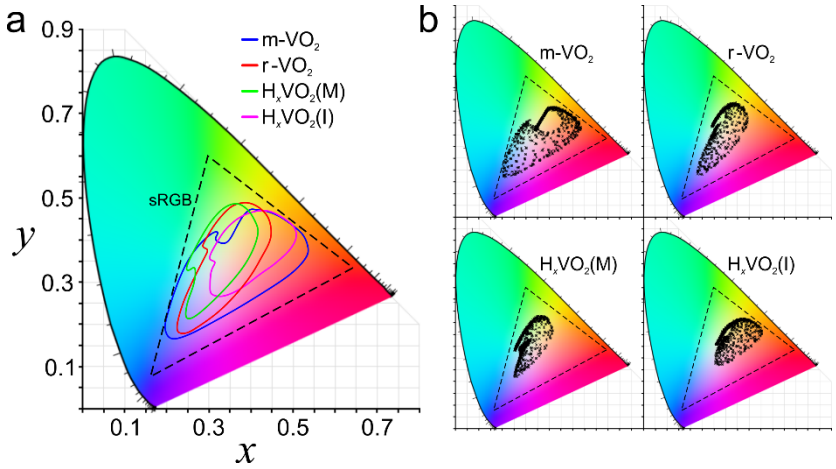

Figure S11 | a, Colour range of the palette from Fig. 2c in the main text at the four states. The black triangle indicates the standard RGB color (sRGB) range. **b**, CIE 1931 chromaticity diagram overlaid with all the colours from the palette. The CIE illuminant D65 is used for the conversion to the chromaticity coordinate. Each black cross in the CIE map indicates a colour square from the palette.

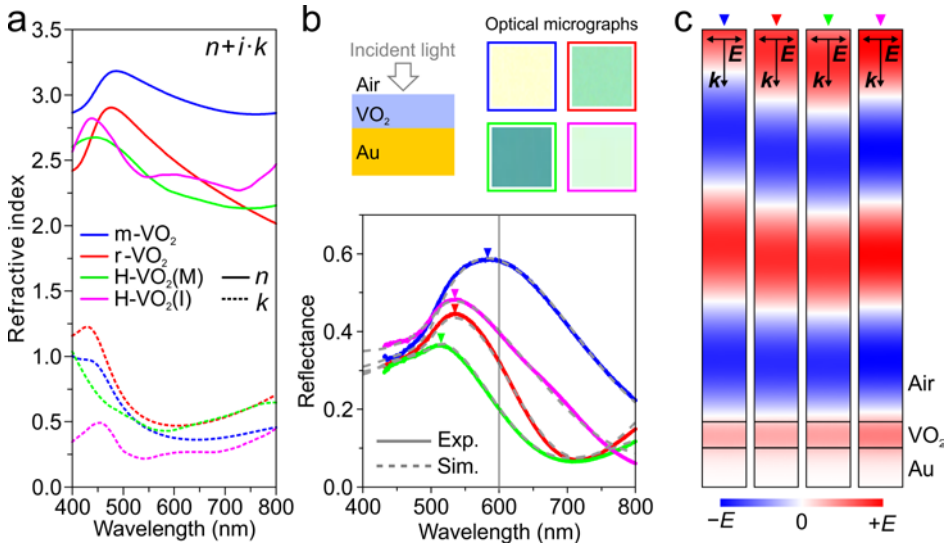

Figure S12 | a, Refractive index ($n + i{\cdot}k$) of the VO_2 at four different phases. The data is from the combination of spectroscopic ellipsometry and reflectance measurements. **b,** Experimental (coloured solid lines) and simulated (gray-dotted lines) reflectance spectra, and the corresponding optical micrographs (10×10 μm^2) of the VO_2 film at four different phases. **c**, The corresponding electric field distributions at the reflectance peaks in **b** (indicated by arrows). Here, a linearly polarized TEM beam is normally incident on the VO_2 surface.

Movie S1

(Gogh, Vincent van (1853-1890): *The Starry Night*, 1889. New York, Museum of Modern Art (MoMA). Oil on canvas, 29 × 36 OE (73.7 × 92.1 cm). Acquired through the Lillie P. Bliss Bequest. Acc. no.: 472.1941. © 2020. Digital image, The Museum of Modern Art, New York/Scala, Florence.)

Hydrogenation and dehydrogenation dynamics of VO_2.

1. High temperatures ($T > T_c$)

At high temperature (100 °C) as shown in Figure S5a, for light H-doping R_{600} first decreases and then approaches a constant at R_{600} = 0.20 (green line) in approximately 40 min. During dehydrogenation by oxygen exposure, the initial r-VO_2 state is restored (R_{600} = 0.32). To verify the dehydrogenated state of r-VO_2, the sample is cooled down to 30 °C in nitrogen. R_{600} returns to 0.58 along the path '③→④→①' as shown in Figure S5a.

To explore further hydrogenation (heavy H-doping), the VO_2 sample is reset to r-VO_2 at 100 °C and loaded with hydrogen until saturation. As shown in Figure S5c, R_{600} decreases rapidly and reaches the H-VO_2(M) state within 40 min as known from light H-doping (Figure S5b). Then, R_{600} increases slowly and eventually approaches 0.40 (magenta line) in 14 hours, indicating the H-VO_2(I) phase has achieved (corresponding to the path '③→⑤→⑧'). Upon oxygen exposure, R_{600} = 0.40 returns to 0.32 in 30 min and r-VO_2 is formed again (path '⑧→③'). The dehydrogenation process is asymmetric to the hydrogenation process and consistent with previous studies.[2]

2. Intermediate temperatures ($T \approx T_c$)

(De)hydrogenation at temperatures close to T_c shows a more complex behaviour. The temperature is kept at 60 °C (two states, '②' and '④' in Figure S6a). Upon hydrogen loading, R_{600} of both the (m/r-VO_2)$_\uparrow$ and (m/r-VO_2)$_\downarrow$ initial states decreases rapidly, and then approaches the H-VO_2(M) phase in 6 hours. As dehydrogenation starts upon oxygen exposure, the reflectance increases gradually and approaches the (m/r-VO_2)$_\downarrow$ state eventually. Similar to the high temperature regime, heavy hydrogenation resulting in the H-VO_2(I) phase can also be achieved. In a subsequent dehydrogenation of VO_2 at 60 °C, H-VO_2(I) returns to (m/r-VO_2)$_\downarrow$ directly, which is again asymmetric to the hydrogenation process (see Figure S7).

3. Low temperatures ($T < T_c$)

For (de)hydrogenation of VO_2 at low temperature (40 °C), upon hydrogen loading, R_{600} (blue line in Figure S8) approaches 0.2 after ~30 hours, corresponding light hydrogenation from m-VO_2 to H-VO_2(M) along the path '①→⑦'. Upon oxygen exposure, R_{600} reaches 0.58 and the initial m-VO_2 state is restored after ~170 hours.

Experimental Section

VO_2 film preparation: VO_2 films (60 nm) were deposited by radio frequency (RF) magnetron sputtering on Au (100 nm)/silicon substrates, in an Angstrom Amod system containing a two-inch diameter vanadium metal target (99.9%). The pressure during the deposition was kept at 6 mTorr (20 sccm Ar and 1 sccm O_2), and the substrates were maintained at room temperature.[3] After deposition, the samples were annealed in a tube furnace under 250 mTorr O_2 (adjusted by flow rate, ~17 sccm) at 450 °C for 10 min.

Hydrogenation and dehydrogenation: Nano-sized Pd dots were formed on the VO_2 films by electron-beam evaporation of Pd (0.5 nm) and subsequent thermal annealing (200 °C in N_2 for 30 min) to achieve hydrogenation at ambient temperatures. Hydrogenation and dehydrogenation were carried out in a laboratory-built gas chamber with a temperature controller (rate 0.1 °C/s, range 20 ºC – 120 °C, accuracy ±0.1 °C). The flow rates of the gases (20 vol.% H_2 in N_2 or 20 vol.% O_2 in N_2) were 1.0 L min^{-1}.

Nanostructure fabrication: The samples were manufactured using electron-beam lithography (EBL). First, a double-layer of PMMA resist (250k-2.5% and 950k-1.5%, Allresist) was spin-coated (5 s at 3000 r.p.m and 30 s at 8000 r.p.m.) on a VO_2 substrate, followed by baking (4 min at 150 °C) on a hotplate in air. EBL (Raith eLine Plus) was performed with 20 kV acceleration voltage, 20 μm aperture, 130 pA current, and 500 μC cm^{-2} dose. After development (90 s in MIBK and 60 s in isopropanol), 30 nm Al_2O_3 and 30 nm Al layers were successively deposited on the substrate using electron-beam evaporation (PFEIFFER Vacuum, PLS-500), followed by a lift-off process in acetone at room temperature for 6 hours. To stabilize the samples, baking at 120 °C was carried out in air for 1 hour after fabrication.

Optical measurements: The optical images and reflectance spectra were measured using a NT&C bright-field reflection microscopy setup with a white light source (Energetiq EQ-99). A digital CCD camera (Allied-Vision Prosilica GT2450C) was used to capture the colour micrographs with a 20 × objective (NA = 0.4). The measured reflectance spectra were normalized with respect to that of an Al mirror.

Numerical simulations: Numerical simulations were carried out using COMSOL Multiphysics software based on a finite-element method. Periodic boundary conditions and waveguide port boundary conditions were used in the simulations. The dielectric constants of Au, Al, and Al_2O_3 were taken from Palik.[4] The refractive indices of VO_2 at the four different phases are shown in Figure S12.

First-principles calculations: The first-principle calculations were performed by using the Vienna *ab initio* simulation package (VASP) code.[5] The exchange and correlation terms were

described using general gradient approximation (GGA) in the scheme of Perdew-Burke-Ernzerhof (PBE).[6] Considering the V-3*d* orbitals, the Hubbard on-site repulsion *U* was applied with the PBE functional to treat the strong-correlation effects.[7] The effective value ($U_{eff} = U-J$) of the on-site Coulomb and exchange strength was 3.4 eV.[8] The valence electron configurations for V, O, Cr and Pt were considered as $3d^3 4s^2$, $2s^2 2p^4$, $3d^5 4s^1$ and $5d^9 6s^1$, respectively. The energy cutoff for the plane-wave was set to 520 eV. The slab model methods were used to model the VO_2 surface and metal-VO_2 interface, and the 4 × 4 × 1 Monkhorst-Pack *k*-point mesh was used. For calculations of the electronic density of states, 8 × 6 × 2 *k*-point mesh was used. This set of parameters were used to ensure that the total energies converged to 10^{-5} eV/unit cell. The Hellmann-Feynman forces were converged to less than 0.01 eV/Å.

(1) Appavoo, K.; Lei, D. Y.; Sonnefraud, Y.; Wang, B.; Pantelides, S. T.; Maier, S. A.; Haglund, R. F., Jr. *Nano Lett.* **2012,** 12, 780–786.
(2) Yoon, H.; Choi, M.; Lim, T.-W.; Kwon, H.; Ihm, K.; Kim, J. K.; Choi, S.-Y.; Son, J. *Nat. Mater.* **2016,** 15, 1113–1119.
(3) Marvel, R. E.; Harl, R. R.; Craciun, V.; Rogers, B. R.; Haglund, R. F., Jr. *Acta Mater.* **2015,** 91, 217–226.
(4) Palik, E. D., *Handbook of optical constants of solids.* Academic Press: New York, 1998.
(5) Kresse, G.; Joubert, D. *Phys. Rev. B* **1999,** 59, 1758–1775.
(6) Perdew, J. P.; Burke, K.; Ernzerhof, M. *Phys. Rev. Lett.* **1996,** 77, 3865–3868.
(7) Wang, L.; Maxisch, T.; Ceder, G. *Phys. Rev. B* **2006,** 73, 195107.
(8) Zhang, J.; He, H.; Xie, Y.; Pan, B. *Phys. Chem. Chem. Phys.* **2013,** 15, 4687–4090.